Acta Biochim Biophys Sin 2011, 43: 556–567 | © The Author 2011. Published by ABBS Editorial Office in association with Oxford University Press on behalf of the Institute of Biochemistry and Cell Biology, Shanghai Institutes for Biological Sciences, Chinese Academy of Sciences. DOI: 10.1093/abbs/gmr042.
Advance Access Publication 2 June 2011

Original Article

# Cucurbitacin B induces rapid depletion of the G-actin pool through reactive oxygen species-dependent actin aggregation in melanoma cells

Yanting Zhang[1†], Dongyun Ouyang[1†], Lihui Xu[2], Yuhua Ji[1], Qingbing Zha[1], Jiye Cai[3], and Xianhui He[1*]

[1]Institute of Tissue Transplantation and Immunology, Jinan University, Guangzhou 510632, China
[2]Institute of Bioengineering, Jinan University, Guangzhou 510632, China
[3]Department of Chemistry, Jinan University, Guangzhou 510632, China
[†]These authors contributed equally to this work.
*Correspondence address: Tel: +86-20-85220679; Fax: +86-20-85221337; E-mail: thexh@jnu.edu.cn

**Cucurbitacin B (CuB), a triterpenoid compound isolated from *Cucurbitaceae* plants, has been reported as a promising anti-cancer agent, yet its action mechanism is still controversial. In this study, we explored the potential mechanism of CuB in murine B16F10 melanoma cells. Anti-proliferation and anti-invasion effects were assessed in cultured cells, and *in vivo* anti-tumor activity was evaluated in a murine subcutaneous melanoma model. Flow cytometry was adopted to analyze cell cycle distribution and reactive oxygen species (ROS) levels. Actin levels were determined by western blot analysis, and the profiles of differential expressed proteins were identified by a quantitative proteomic approach. The results showed that CuB exerted inhibitory effects on cell proliferation, colony formation, as well as migration and invasion potential of the melanoma cells. The growth of subcutaneous melanoma was significantly inhibited in mice treated with CuB when compared with control group. Furthermore, CuB treatment caused rapid cell membrane blebbing and deformation, and induced $G_2$/M-phase arrest and formation of multiploid cells. Notably, the G-actin pool was rapidly depleted and actin aggregates were formed quickly after CuB treatment. A number of cytoskeleton-regulatory proteins were differentially regulated. Blockage of ROS production significantly reduced the G-actin depletion ability and the anti-tumor activity of CuB. These findings indicate that CuB induces rapid depletion of the G-actin pool through ROS-dependent actin aggregation in melanoma cells, which may at least partly account for its anti-tumor activity.**

*Keywords* cucurbitacin B; melanoma; G-actin; actin aggregation; reactive oxygen species

Received: March 3, 2011 Accepted: April 7, 2011

## Introduction

Cucurbitacin B (CuB) is a triterpenoid compound isolated from *Cucurbitaceae* plants that have been used as anti-inflammatory, anti-diabetic and abortifacient medicines for centuries in China [1–4]. Recently, accumulating evidence indicates that CuB and its relatives inhibit the growth of a wide spectrum of human malignant cells both *in vitro* and in xenografted tumor models, including breast cancer, glioblastoma multiforme, myeloid leukemia, pancreatic cancer, laryngeal cancer, and melanoma cells [5–11]. Although the anti-tumor mechanism of CuB has been investigated extensively, there are several controversies among different studies. For example, some studies have shown that CuB acts as a dual inhibitor of Jak2 and signal transducers and activators of transcription 3 (STAT3) [9,10,12–14], whereas other reports have suggested that CuB and its relatives exhibit anti-tumor effects independent of STAT3 [15–17]. In addition, one study indicates that CuB activates Erk1/2 [18], whereas the other demonstrates that CuB inhibits Erk1/2 phosphorylation [7]. These contradictory results make the action mechanism of CuB quite controversial and further investigations are warranted to clarify this issue.

One intriguing finding is that CuB induces cell cycle arrest at the $G_2$/M phase and formation of multiploid cells. For instance, CuB causes rapid disruption of microfilaments (F-actin), which is associated with the multinucleation of glioblastoma cells [7]. Similar phenomena of CuB action have also been observed in both breast cancer and leukemia cells [6,8]. More recently, it has been demonstrated that cucurbitacin I inhibits cell motility by indirectly interfering with actin dynamics [19]. Together, these studies suggest that the disruption of actin dynamics may be a critical activity of cucurbitacins including CuB. Yet, the exact mechanism of CuB on the actin cytoskeleton system in cells is still not clearly defined.

In this study, we showed that CuB rapidly depleted the G-actin pool, resulting in actin aggregation in murine melanoma cells. *N*-acetyl-L-cysteine (NAC), a well-known antioxidant and reactive oxygen species (ROS)-scavenger, could significantly reduce both the G-actin depletion ability and the inhibitory activities of CuB in the melanoma cells. These results indicated that CuB induced rapid depletion of the G-actin pool through an ROS-dependent mechanism, which might at least partly account for its antitumor activity in melanoma cells.

## Materials and Methods

### Chemical reagents

CuB (molecular weight 558.7 Da) with 98% purity was obtained from Zhongxin Innova Laboratories (Tanjin, China), dissolved in dimethyl sulfoxide (DMSO) at 10 mM, and stored at −20°C. Triton X-100, sucrose, sodium deoxycholate, NAC, dithiothreitol (DTT), propidium iodide, and DMSO were from Sigma-Aldrich (St Louis, USA). RNase A was purchased from Invitrogen (Carlsbad, USA).

### Cell culture

Mouse B16F10 cell line was obtained from the Cell Bank of the Chinese Academy of Sciences (Shanghai, China) where routine cell line authentication using isoenzyme assay is performed, cultured in DMEM (Invitrogen) supplemented with 10% fetal bovine serum (Invitrogen), 100 U/ml penicillin, and 100 μg/ml streptomycin (Invitrogen), and maintained at 37°C in a humidified incubator of 5% $CO_2$.

### Measurement of cell proliferation and viability

The effect of CuB on the proliferation of B16F10 cells was measured using MTS assay (CellTiter 96 Aqueous ONE Solution kit; Promega, Madison, USA). The cells were seeded into 96-well plates at $5 \times 10^3$ cells per well (100 μl) for 24 h. On the next day, the medium were replaced with fresh medium containing different concentrations of CuB or vehicle (DMSO). After incubation for additional 48 h, MTS (20 μl) was added to each well and incubated at 37°C for 1−4 h. The absorbance at 490 nm was measured using a microplate reader (Model 680; Bio-Rad, Richmond, USA). Three independent experiments were performed, each in triplicates. The 50% inhibition concentrations ($IC_{50}$) indicated the concentration corresponding to 50% reduction of cell proliferation as compared with the control.

### Murine tumor model and tumor therapy

Female C57BL/6 mice (6−8 weeks old) were supplied by the Experimental Animal Center of Southern Medical University (Guangzhou, China). Animal experiments were conducted in accordance with the guidelines of Jinan University (Guangzhou, China) and the National Institutes of Health (NIH). Tumor model was performed as previously reported [20]. In brief, B16F10 cells in the logarithmic growth phase were used for injection. The cells were kept on ice and mixed well prior to each injection. The mice (eight for each group) were injected with $1 \times 10^5$ tumor cells subcutaneously on the right side. Treatment was started the day after cell implantation with either 1 mg/kg body weight intraperitoneal injections of CuB thrice a week (treatment group) or diluent control alone (control group). Tumor size was measured with calipers every 3 days starting from the eighth day after tumor injection. Tumor volume was determined by the following formula: tumor volume ($mm^3$) = $1/2 \times A$ (mm) × $B^2$ ($mm^2$), where '*A*' represent the largest dimension of the tumor and '*B*' indicates the smallest dimension [21].

### Measurement of colony-formation potential

Colony-formation assay was performed as follows. One thousand cells were seeded in 60-mm Petri dishes and incubated for 5 days in the presence or absence of 1 μM CuB. Then the cells were stained with methylene blue (0.5%, *w*/*v* in 50% methanol) and images were taken using FluorChem SP imaging system (Alpha Innotech, San Leandro, USA). The colony cells were also photographed under a microscope (Nikon, Tokyo, Japan).

### Cell cycle analysis

B16F10 cells seeded in six-well plates were incubated with CuB for 24, 48 and 72 h. Both detached and attached cells were harvested and washed twice with cold phosphate-buffered saline (PBS). After fixation in 70% cold ethanol at −20°C for at least 1.5 h, the samples were treated with staining solution (RNase A, 30 μg/ml; propidium iodide, 50 μg/ml) at 37°C for 1 h, and then analyzed by a flow cytometer (FACSCalibur; Becton Dickinson, Mountain View, USA).

### Cell migration assay

Scratch wound-healing assay was performed to determine cell migration using confluent cultures (80%−90% confluence). Cells were photographed under a microscope at 0, 24 and 48 h. The wound width in terms of pixels was quantitated with PhotoShop V8.0 (Adobe, San Jose, USA).

### Matrigel invasion assay

The *in vitro* invasion assay was carried out in chambers (Transwell; Corning, Cambridge, USA) coated with a thin layer of Matrigel (Becton Dickinson). Matrigel was diluted in serum-free DMEM to 0.5 mg/ml and the upper chamber was coated with 100 μl gel suspension for 1 h at 37°C. Cells were added to the upper chamber at $1 \times 10^4$ in 100 μl of serum-free DMEM and the chambers were

placed into a 24-well plate containing 0.5 ml/well complete medium. After 48 h of incubation, the cells on the upper membrane surface were gently removed and the lower membrane surfaces were stained with 0.1% crystal violet in 20% methanol. Stained cells were photographed under a microscope (Nikon).

### Extraction of soluble actins and insoluble actin filaments

Soluble actins (G-actin) were extracted as described previously [22]. Briefly, cells were washed twice with cold (4°C) PBS after exposure to CuB or vehicle (control), and the cells were kept on ice. G-actins were extracted with soluble actin extraction solution [50 mM Tris-HCl, pH 7.4, 300 mM sucrose, 25 mM NaCl, 2 mM ethylene glycol tetraacetic acid (EGTA), 5 mM $MgCl_2$, 0.2% Triton X-100, 25 mM sodium fluoride, 1 mM sodium orthovanadate, 1 mM phenylmethylsulfonyl fluoride (PMSF), and protease inhibitor cocktail from Roche (Mannheim, Germany)]. The main cytoskeletal framework containing microfilaments remained attached to the dishes. After washing the dishes once more with soluble actin extraction solution, the Triton-insoluble cytoskeleton was scraped off from the dishes in 500 μl of strong RIPA [50 mM Tris-HCl, pH 7.4, 1% Triton X-100, 1% sodium deoxycholate, 0.1% sodium dodecyl sulfate (SDS), 150 mM NaCl, 1 mM ethylenediaminetetraacetic acid (EDTA), 0.1 mM DTT, 25 mM sodium fluoride, 1 mM sodium orthovanadate, 1 mM PMSF, and protease inhibitor cocktail from Roche] and saved on ice. These samples were vortexed vigorously and spun in a microcentrifuge for 5 min at 4°C. The supernatants that contained the cytoskeletal F-actin fraction were stored at −70°C. The residual pellets were further lysed with 2× SDS-polyacrylamide gel electrophoresis (PAGE) loading buffer containing 200 mM DTT.

### Quantitative proteomic analysis

Cells were seeded in 75 $cm^2$ flasks and treated with vehicle or 1 μM CuB for 24 h. Subsequently, the cells were washed thoroughly with ice-cold PBS and followed by lysis with 0.5 ml RIPA (Pierce, Rockford, USA). Quantitative proteomic analysis was performed essentially as described previously [23]. In this study, three biological replicates were carried out. The differential regulation cutoff was set at 1.5 folds. Ratio>1.50 or <0.67 was considered as differentially up- and down-regulated, respectively.

### Analysis of ROS production

ROS level within cells was determined by flow cytometry using $H_2$DCF-DA (Molecular Probes, Eugene, USA), an ROS-sensitive fluorescent compound that can readily diffuse into cells and be hydrolyzed by intracellular esterase to form $H_2$DCF within cells. The latter is then oxidized by ROS, if there were, to produce fluorescent compound dichlorofluorescein (DCF). In this study, we first stained B16F10 cells with $H_2$DCF-DA (10 μM) for 30 min, and then treated the cells with CuB for 1 h. ROS level in cells was analyzed using a flow cytometer (FACSCalibur).

### Western blot analysis

Cell lysates were prepared by lysing PBS-washed cells with RIPA buffer (Beyotime, Haimen, China) containing 1% Nonidet P-40, 0.5% sodium deoxycholate, 0.1% SDS, 50 mM Tris-HCl, pH 7.4, supplemented with NaF, $NaVO_4$, EDTA and protease inhibitor cocktail (Roche). The 40 or 10 μg of total proteins were separated by SDS-PAGE followed by electro-transfer to polyvinylidene difluoride membrane. Membranes were immunoblotted with antibodies against β-tubulin and pan-actin (Santa Cruz Biotechnology Inc., Santa Cruz, USA) and detected with enhanced chemiluminescence kit (BeyoECL Plus; Beyotime).

### Statistical analysis

Data were expressed as the mean ± SD. Statistical analysis was performed using GraphPad Prism 4.0 (GraphPad Software Inc., San Diego, USA). One-way ANOVA, followed by Dunnett's multiple comparison test (versus control), was used to analyze the statistical significance among multiple groups. $P$ values <0.05 were considered statistically significant.

## Results

### CuB exhibited significant anti-tumor activity in murine melanoma cells

CuB inhibited the proliferation of B16F10 cells in a dose-dependent manner with an $IC_{50}$ value of 0.32 ± 0.04 μM [**Fig. 1(A)**] . Cell cycle analysis showed that CuB treatment arrested cells in $G_2$/M phase and markedly increased the multiploid cell numbers [**Fig. 1(B)**]. As shown in **Fig. 1(B)** (upper panel), treatment with 1 μM of CuB did not effectively prevent tetraploid cells (4N) from entering their S phase and $G_2$/M phase (DNA content >4N), thus the percentages of cells with DNA content >4N were gradually increased after CuB-exposure. About 6% cells had >4N DNA content at 24 h, whereas >20% cells had >4N DNA content at 72 h [**Fig. 1(B)**, bottom panel]. When CuB was washed out after 48 h incubation and the cells were cultured for another 48 h, a larger number of multinucleated cells were formed [**Fig. 1(C)**]. Time lapse analysis revealed that cell membrane blebbing appeared immediately after exposure of cells to CuB and the cells deformed rapidly [**Fig. 1(D)**], suggesting a quick disruption of cortex

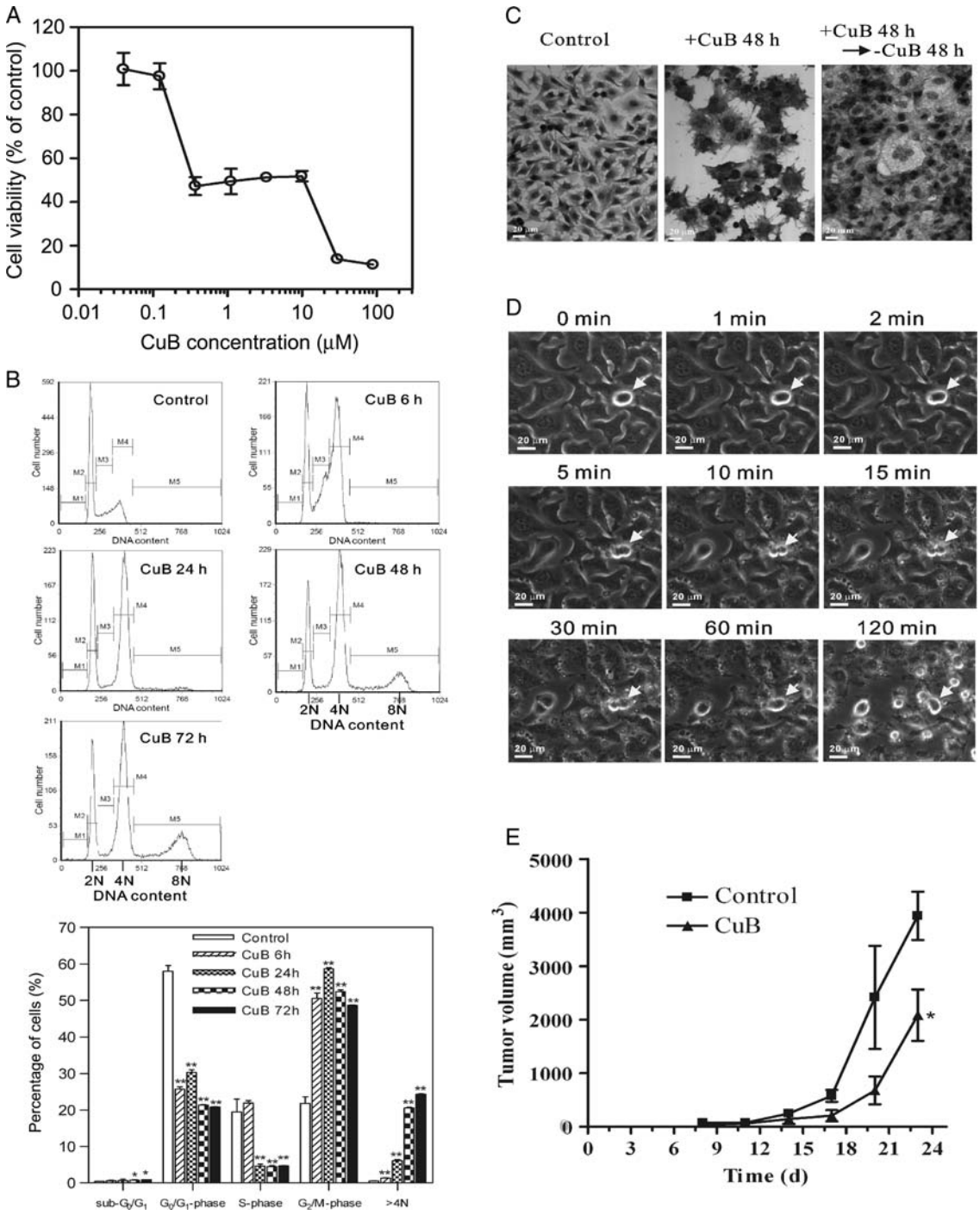


**Figure 1 CuB induced substantial changes in a variety of cellular behaviors of murine melanoma cells** (A) Analysis of proliferation of B16F10 cells exposed to CuB for 48 h via MTS assay. (B) Cell cycle distribution in B16F10 cells after treatment with CuB (1 μM) for different times. Representative flow cytometry plots of three independent experiments were performed (upper panel) and data are presented as mean ± SD (bottom panel). The 2N, 4N, and 8N indicate the DNA contents of diploid, tetraploid and 8-ploid cells, respectively. M1, sub-$G_1/G_0$; M2, $G_1/G_0$; M3, S; M4, $G_2$/M; M5, >4N. (C) Morphology of the cells after 1 μM CuB treatment (hematoxylin and eosin staining). (D) Time lapse analysis of rapid blebbing induced by CuB (1 μM) treatment. Arrows indicate the cell undergoing cytokinesis. (E) Inhibition of the growth of subcutaneous melanoma in C57BL/6 mice. The mice (eight for each group) were injected with $1 \times 10^5$ tumor cells subcutaneously on the right side. CuB (1 mg/kg three times a week) or vehicle was given intraperitoneally from the day after cell implantation. Tumor size was measured with calipers every 3 days starting from the eighth day after tumor injection. $^*P < 0.05$; $^{**}P < 0.01$.

actin cytoskeleton. We also observed that the contractile ring, which had already been formed prior to the addition of CuB, could still work even though cytokinesis could not finally be fulfilled [**Fig. 1(D)**, the cell marked with an arrow was undergoing cytokinesis]. We also determined whether CuB administration could suppress the growth of

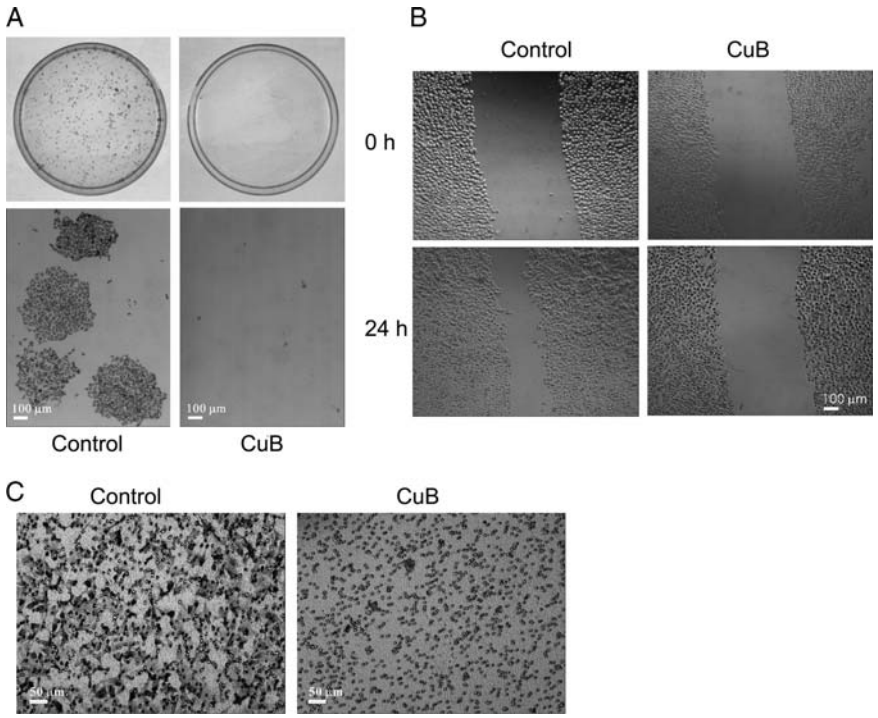


**Figure 2 CuB exhibited anti-invasive effect on murine melanoma cells** CuB concentration was 1 μM. (A) Colony formation of B16F10 cells cultured for 5 days in the absence or presence of CuB. Upper panels show the foci in culture dishes and bottom panels show the foci morphology. (B) Wound-healing assay of the confluent B16F10 cells in the presence or absence of CuB. Wound healing was analyzed by comparing the images taken at 0 and 24 h. (C) Invasion potential of B16F10 cells through Matrigel-coated transwell after 48 h of treatment with CuB. All experiments were repeated twice with duplicates.

melanoma *in vivo*. B16F10 cells were subcutaneously implanted in normal mice, and the experimental mice were given 1 mg/kg body weight of CuB intraperitoneally thrice a week. The growth of tumors was significantly inhibited in the mice treated with CuB when compared with the control mice [**Fig. 1(E)**].

We then examined whether CuB could inhibit the invasive ability of B16F10 cells. As shown in **Fig. 2(A)**, colony-formation ability was totally blocked by CuB treatment. The effect of CuB on cell migration was tested using scratch assay. Incubation of 1 μM of CuB almost completely blocked the wound-healing ability within 24 h [**Fig. 2(B)**]. Furthermore, matrigel-coated transwell assay showed that the invasion ability was also completely inhibited by CuB treatment [**Fig. 2(C)**]. These results demonstrated that CuB could markedly inhibit the migration and invasion ability of B16F10 cells.

### Rapid depletion of the G-actin pool was induced in CuB-treated melanoma cells

Based on the above observations, we focused our interest on the actin dynamics of CuB-treated cells. Soluble and insoluble actins (microfilament cytoskeleton) in CuB-treatment samples were sequentially extracted by soluble actin extraction solution (containing 0.2% Triton X-100) and strong RIPA. The Triton-soluble fraction (referred as the G-actin pool) mainly contains G-actin monomers and the RIPA-soluble actins stand for F-actin microfilaments. Both SDS-PAGE and western blot analysis revealed that the G-actin pool (protein band at 43 kDa) was rapidly depleted within 30 min after CuB treatment and then slowly increased, but it did not recover back to normal level even after 24 h [**Fig. 3(A)**, left panel]. The RIPA-soluble F-actins were stable during the course of experiment [**Fig. 3(A)**, right panel]. In addition, β-tubulin levels in Triton-extracted fraction were not affected by CuB [**Fig. 3(A)**, left panel] and slightly increased in the RIPA-soluble fraction [**Fig. 3(A)**, right panel].

As revealed by directly lysing the cells with 2× SDS-PAGE loading buffer and western blot analysis, the levels of total actins were equal both in control and in CuB-treated cells [**Fig. 3(B)**], indicating that CuB treatment changed the distribution rather than the total amount of actins. It seemed that CuB had induced the formation of actin aggregates that were insoluble in strong RIPA. Thus, the RIPA-insoluble residues were further extracted with 2× SDS-PAGE loading buffer. As shown in **Fig. 3(B)**, a higher level of actins was detected in the residues of CuB-treated cell samples, which indicated that in these cells the majority of G-actins were recruited to form RIPA-insoluble aggregates. In these aggregates, actin filaments might have been cross-linked by disulfide bonds because more actins were extracted with RIPA containing 50 mM of DTT than that without DTT [**Fig. 3(C)**].

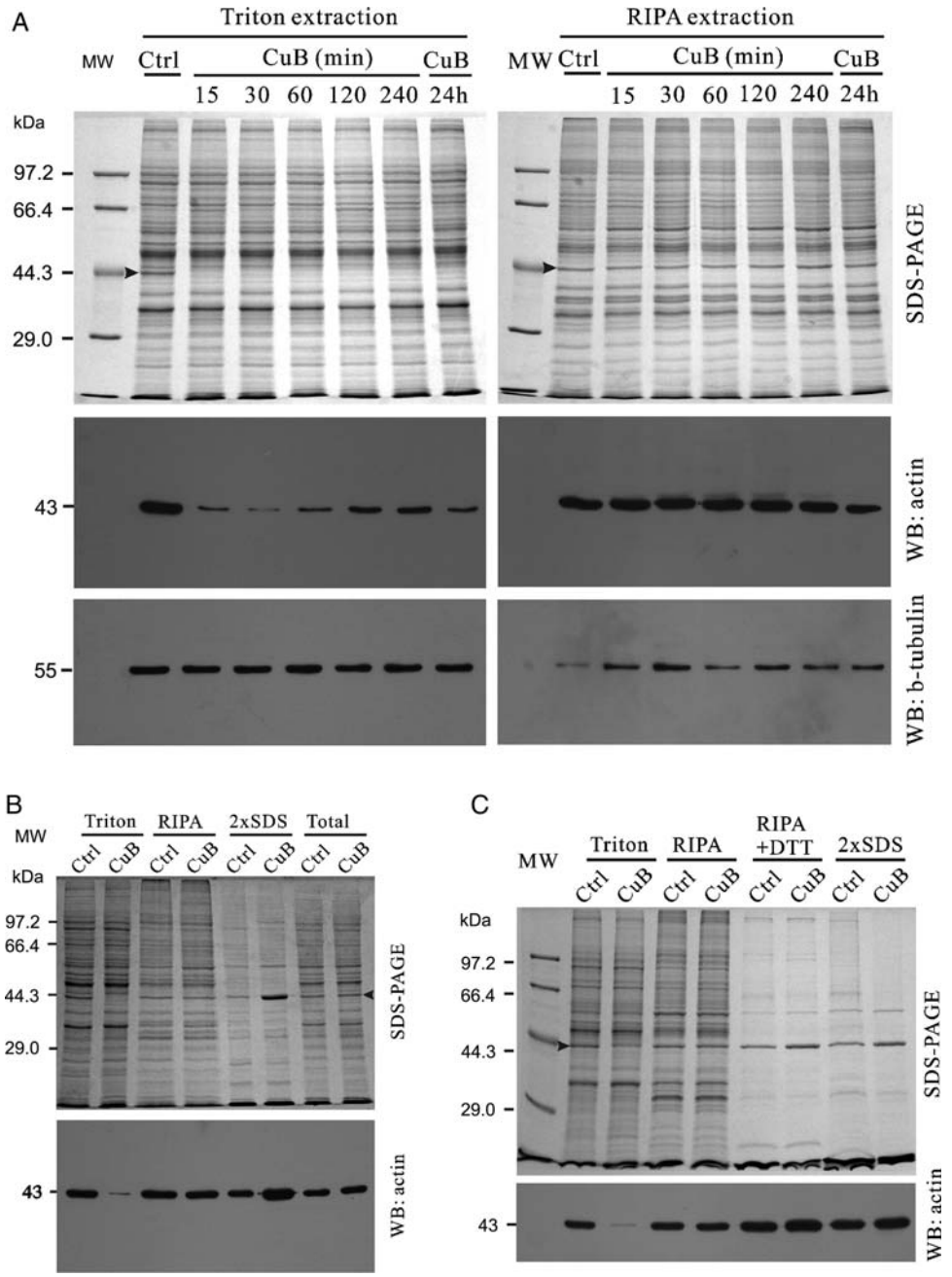


**Figure 3 CuB induced rapid depletion of the G-actin pool in murine melanoma cells** The concentration of CuB was 1 μM for all experiments. (A) Representative SDS-PAGE (up) and western blot analysis (middle) showing Triton-soluble (G-actin) and RIPA-soluble actin (F-actin) levels in 10 μg of total proteins from the cells treated with CuB for different time points. Western blot for β-tubulin is also shown (bottom). For details see Materials and Methods. (B) Actins in different extracted fractions of cells treated with CuB for 30 min. The cells were sequentially extracted with Triton, strong RIPA and finally 2× SDS-PAGE loading buffer. 'Total' in this figure represents lysing cells directly with 2× SDS-PAGE loading buffer. Ten micrograms of proteins were loaded to each lane. (C) Actins in sequential extraction fractions. Proteins were sequentially extracted with Triton, RIPA and RIPA containing 50 mM DTT. Ten micrograms of proteins were loaded to each lane. Arrowheads indicate the position of actin in SDS-PAGE gels. Ctrl: control.

## Microfilament-regulatory proteins were differentially expressed in CuB-treated melanoma cells

Next we checked the protein expression profiles of CuB-treated cells. Cells were treated with CuB for 24 h, and then proteins were analyzed by a quantitative proteomic approach. The results showed that a total of 124 proteins were up-regulated and 86 proteins were down-regulated by CuB (data not shown). The differentially expressed actin cytoskeleton components and regulators were listed in **Table 1**. Notably, F-actin-severing factors (such as Dstn, Wdr1 and Cfl1) were greatly up-regulated in the CuB-treated group, whereas those promoting actin

**Table 1 Differentially expressed cytoskeleton-related proteins in B16F10 cells treated with CuB[a]**

| Gene symbol | Protein name | CuB/Control | |
|---|---|---|---|
| | | Mean | SD |
| Up-regulated | | | |
| Myl9 | Myosin-regulatory light polypeptide 9 | 6.66 | 0.82 |
| Csrp1 | Cysteine and glycine-rich protein 1 | 5.34 | 0.68 |
| Tpm1 | Tropomyosin alpha-1 chain isoform 4 | 4.46 | 0.74 |
| Dstn | Destrin | 4.00 | 2.46 |
| Zyx | Zyxin | 3.61 | 0.64 |
| Tpm4 | Tropomyosin alpha-4 chain | 3.02 | 0.06 |
| Myl6 | Isoform Smooth muscle of Myosin light polypeptide 6 | 2.57 | 0.73 |
| Vcl | Vinculin | 2.52 | 1.24 |
| Myh9 | Myosin-9 | 2.41 | 0.65 |
| Cnn2 | Calponin-2 | 2.35 | 0.35 |
| Nes | Isoform 1 of Nestin | 2.34 | 0.098 |
| Actn1 | Alpha-actinin-1 | 2.31 | 0.28 |
| Wdr1 | WD repeat-containing protein 1 | 2.25 | 0.36 |
| Ywhah | 14-3-3 protein eta | 2.07 | 0.57 |
| Flna | Filamin, alpha | 2.02 | 0.46 |
| Tagln2 | Transgelin-2 | 2.00 | 0.40 |
| Calr | Calreticulin | 1.77 | 0.27 |
| Vasp | Vasodilator-stimulated phosphoprotein | 1.58 | 0.64 |
| Cfl1 | Cofilin-1 | 1.57 | 0.30 |
| Vim | Vimentin | 1.54 | 0.29 |
| Down-regulated | | | |
| Dbn1 | Isoform A of Drebrin | 0.14 | 0.07 |
| Cttn | Src substrate cortactin | 0.17 | 0.07 |
| Spna2 | Isoform 1 of Spectrin alpha chain, brain | 0.24 | 0.08 |
| Actb | Actin, cytoplasmic 1 | 0.27 | 0.06 |
| Krt76 | Keratin, type II cytoskeletal 2 oral | 0.39 | 0.17 |
| Spnb2 | Isoform 1 of Spectrin beta chain, brain 1 | 0.43 | 0.19 |
| Stmn1 | Stathmin | 0.55 | 0.01 |
| Arpc3 | Actin-related protein 2/3 complex subunit 3 | 0.56 | 0.05 |
| Arpc2 | Actin-related protein 2/3 complex subunit 2 | 0.57 | 0.01 |
| Marcks | Myristoylated alanine-rich C-kinase substrate | 0.60 | 0.07 |
| Lima1 | LIM domain and actin-binding protein 1 isoform a | 0.62 | 0.38 |
| Krt79 | Keratin, type II cytoskeletal 79 | 0.64 | 0.26 |
| Krt10 | Isoform 1 of Keratin, type I cytoskeletal 10 | 0.66 | 0.06 |

CuB, cucurbitacin B.

[a]The regulation cutoff value was set at 1.5 folds. A protein with an expression level $>1.50$ folds or $<0.67$ folds compared with the control was considered as the differentially expressed one.

polymerization (such as Dbn1, Arpc2 and Arpc3) were decreased significantly, suggesting an over-polymerization of actins occurred within the cells. On the other hand, contractile-related proteins (Myh9, Myl9, Myl6, Tpm1 and Tpm4) and F-actin cross-linking proteins (such as Flna, Actn1, Zyx, Vcl and Vasp) that are required for maintaining the cortex F-actin were also up-regulated, suggesting a dysfunction of cortex actin structure.

## G-actin depletion in CuB-treated cells was suppressed by NAC

As oxidative stress is closely related to the disruption of microfilaments, the influence of ROS on the activity of CuB were evaluated. NAC (10 mM), which is non-toxic to B16F10 cells, was used to block ROS production in the cells. In CuB-treated cells, NAC blocked the inhibitory effects of CuB on the wound-healing ability [**Fig. 4(A)**] and Matrigel invasion potential [**Fig. 4(B)**]. In the colony-

formation assay, NAC could also partially restore the colony-forming ability of CuB-treated cells [**Fig. 4(C)**]. Pretreatment with NAC could almost entirely block the cell cycle arrest induced by CuB [**Fig. 5(A)**]. NAC pretreatment also significantly suppressed CuB-induced cell membrane blebbing [**Fig. 5(B)**]. In most of the microscopic fields, CuB-induced 'blebbing' was no longer observed in cells pretreated with NAC. ROS-level analysis showed that NAC alone had markedly lowered the ROS basal level in the control cells. The ROS level was further lowered when the cells were treated with NAC plus CuB [**Fig. 5(C)**]. Moreover, the G-actin level in CuB and NAC co-treated cells was restored to a relatively higher level when compared with CuB-treated cells [**Fig. 5(D)**]. These data suggested that the basal ROS in B16F10 melanoma cells was necessary for CuB to deplete the G-actin pool and to exhibit other anti-tumor effects.

## Discussion

Cucurbitacin family members represent new kinds of anti-tumor agents and their action mechanism has been extensively investigated. Although many studies have shown that cucurbitacins exhibit inhibitory effect on STAT3 phosphorylation in several human tumor cell lines [5,9,10,12,24,25], accumulated evidence indicates that the disruption of actin cytoskeleton is involved in the immediate events of these compounds [7,8,26,27]. CuB induces quick clumping of F-actin and rapid morphology alteration in glioblastoma multiform, breast cancer [6,7], and myeloid leukemia cells [8]. Many other members of cucurbitacin family have also been shown to affect actin cytoskeleton. For instance, cucurbitacin I, which has been shown to target the Jak2/STAT3 signaling pathway [5], profoundly affects the actin cytoskeleton and may therefore modulate cell morphology, migration, adherence and gene expression in non-tumor cells [17]. In addition, cucurbitacin F induces the formation of actin aggregates in *Drosophila* $K_{c167}$ cells [28], and cucurbitacin E induces the disruption of actin cytoskeleton in prostate carcinoma cells [26]. Cucurbitacin E has also been shown to interact directly with actin and consequently stabilizes the polymerized actin [29]. More recently, it has been reported that cucurbitacin I inhibits cell motility by indirectly interfering with actin dynamics [19]. Consistent with these studies, our data indicated that CuB induced rapid depletion of the G-actin pool through ROS-dependent actin aggregation in murine B16F10 melanoma cells. CuB-induced disturbance of actin dynamics may at least partly account for its inhibitory activities on cell cycle arrest, proliferation, and migration of the melanoma cells.

By the extraction of actins fractionally, we found that the G-actin pool was rapidly depleted and actin aggregates were formed in CuB-treated cells. These aggregates could not be dissolved by strong RIPA without reducing agent but was partially soluble in RIPA with a reducing agent, suggesting that the actin aggregates had been cross-linked by sulfide bonds. As cytoskeleton components (including G-actins and F-actin filaments) are highly dynamic, rapid depletion of the G-actin pool blocks the reorganization of actin cytoskeleton [30], especially the cortex F-actin under plasma membrane and the contractile rings required for normal cytokinesis. In this study, we observed that plasma membrane blebbing was induced immediately and cell motility and invasion ability were also lost after CuB treatment. These phenomena could be explained by CuB-induced G-actin depletion. Different from the action of colchicines (microtubule-targeting drugs), CuB prohibited the cytokinesis without influencing the function of mitotic apparatus. Time lapse analysis revealed that the contractile rings were functional, but the cytokinesis could not be fulfilled, suggesting an inability of the cells to form new cortex F-actin structures for separating the two compartments. Consequently, CuB-treated cells were arrested in $G_2$/M-phase and multinuclear cells were formed. Taken together, these results suggested that CuB exhibited anti-tumor activity by inducing a rapid depletion of the G-actin pool through the formation of cross-linked actin aggregates in B16F10 cells.

Under normal condition, a balance between G-actin and F-actin maintains the homeostasis of cells [30]. Disturbance of the dynamic equilibrium between G-actin and F-actin not only influences the cytokinesis, cell shape, and locomotion, but also changes the expression of actin-regulatory proteins [30,31]. Our proteomic data showed that several F-actin-severing proteins, such as ADF (Dstn), WD repeat-containing protein 1 (Wdr1) and cofilin-1 (Cfl1), were markedly up-regulated, whereas those for actin organization and branching nucleation (Drebrin, Arpc2 and Arpc3) were down-regulated. It is believed that the Arp2/3 complex participates in the assembly of a dense network of short-branched actin filaments, which play an important role in cellular motility [32]. CuB-induced down-regulation of Arp2/3 would decrease branching nucleation and F-actin assembly, leading to decreased cell locomotion. On the other hand, ADF/cofilins enhance F-actin dynamics through binding co-operatively to F-actin, thus initiating fragmentation (severing) of actin filaments [30]. Hence, up-regulation of actin-severing proteins should elevate the G-actin level under physiological condition. Yet, under non-physiological condition, F-actin-severing proteins may enhance the formation of actin aggregates [33]. For example, cells cultured under heat-shock, osmotic-stress, or cofilin-overexpression experimental conditions results in the formation of actin-containing structures called ADF/cofilin rods [33]. Jasplakinolide, a cell membrane-

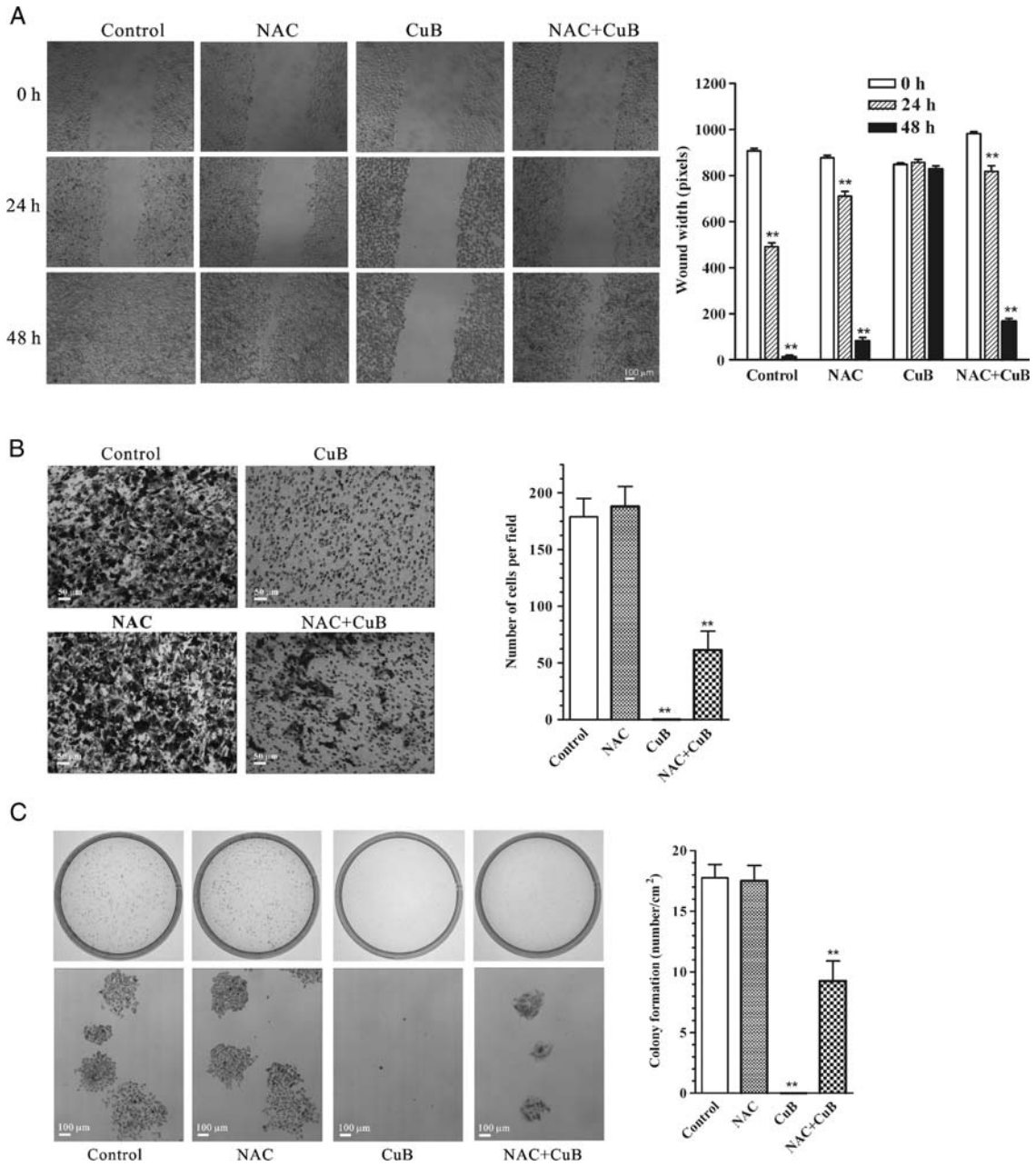


**Figure 4 NAC blocked the inhibitory effects of CuB on invasive potential of murine melanoma cells** NAC (10 mM) was added 1 h before exposure to 1 μM CuB. (A) Wound-healing assay (left) of the confluent B16F10 cells treated with CuB. Data in the histogram (right) are presented as mean ± SD of three independent experiments. (B) Invasion potential of B16F10 cells through Matrigel-coated transwell after 48-h treatment with CuB followed by staining with crystal violet (left). Data in the histogram (right) were presented as mean ± SD. (C) Colony formation of B16F10 cells during the course of 5 days in the absence or presence of CuB. Upper panels show the foci in dishes and bottom panels show the foci morphology (left). Data in the histogram (right) were presented as the mean ± SD. $^{**}P < 0.01$.

permeable toxin, serves as an F-actin stabilizer to induce large F-actin aggregates or inclusion bodies containing β- and γ-actin, ADF/cofilin, cortactin, and the actin nucleator Arp2/3 [34]. Thus, up-regulation of ADF/cofilin might enhance the effect of CuB by the formation of actin-rich aggregates in cells. In addition, several F-actin cross-linking and/or binding proteins (Flna, Actn1, Zyx, Vcl and Vasp) might also enhance the formation of actin aggregates. Take together, the proteomic data indicated that there was a global change in the actin cytoskeleton in the cells after exposure to CuB, which strongly supported our observation of actin dynamics alteration.

Recently, it has been reported that CuB induces $G_2$/M-phase arrest and apoptosis in human colon adenocarcinoma SW480 cells through an ROS-dependent mechanism [15]. It is believed that melanoma cells have diminished antioxidant potential when compared with normal melanocytes, leading to an increase in ROS production and

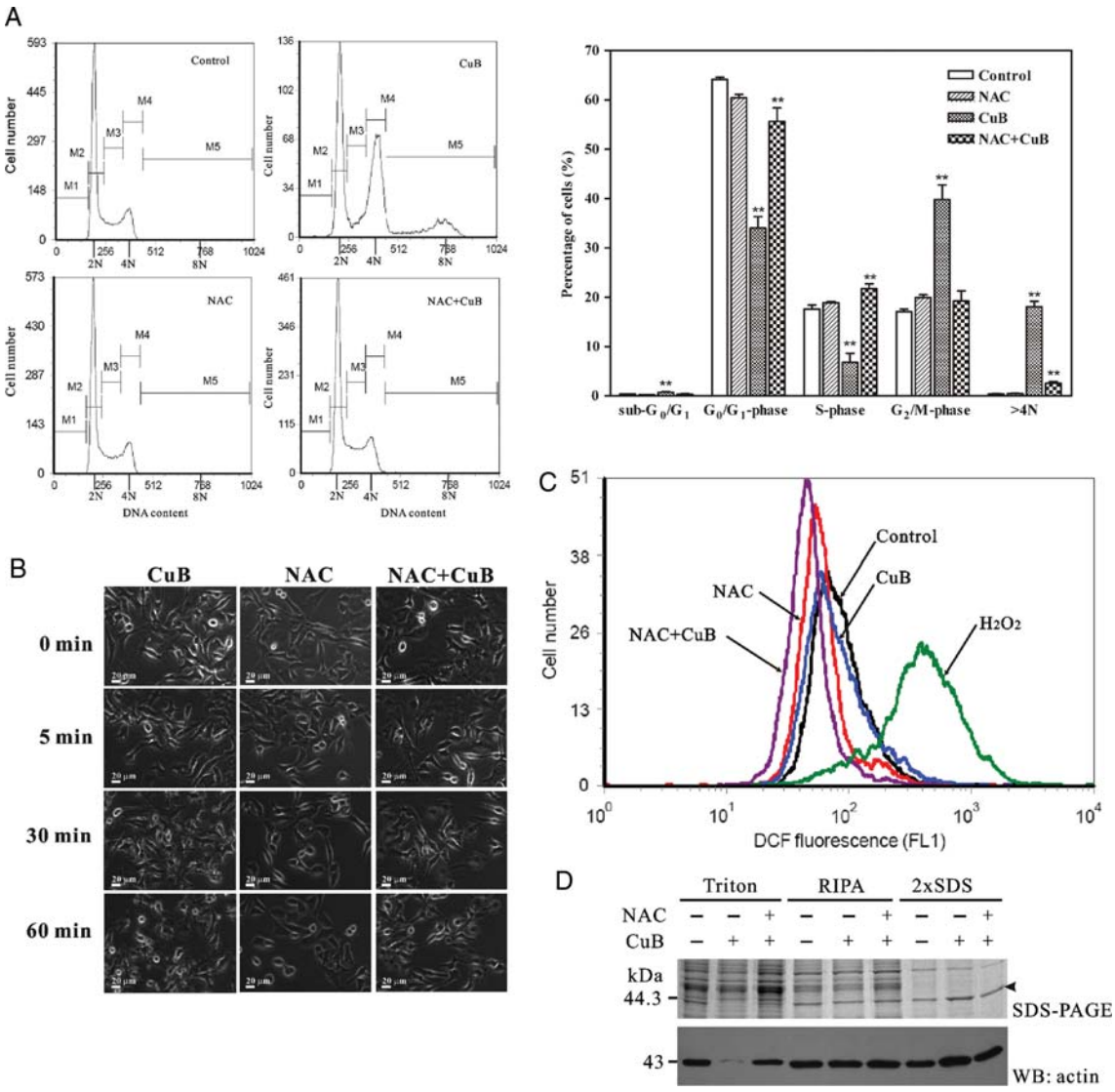


**Figure 5 NAC blocked the effects of CuB on melanoma cells** NAC (10 mM) was added 1 h before exposure to 1 μM CuB. (A) Cell cycle distribution in B16F10 cells after additional 48 h culture. The 2N, 4N, and 8N indicate the DNA contents of diploid, tetraploid, and 8-ploid cells, respectively. M1, sub-$G_1/G_0$; M2, $G_1/G_0$; M3, S; M4, $G_2/M$; M5, >4N. (B) Pretreatment of NAC prevented the membrane blebbing induced by CuB. (C) Analysis of ROS levels in B16F10 cells. Cells were pretreated with NAC and incubated with CuB for 1 h. The experiments were repeated three times. (D) Presence of NAC prevented CuB-induced depletion of the G-actin pool (Triton extracted actins). Cells were exposed to CuB for 30 min with or without NAC pretreatment. Ten micrograms of total proteins were loaded to each lane for both SDS-PAGE and western blot. The arrowhead indicates the position of actin in SDS-PAGE gel. $^{**}P < 0.01$.

impairment of ROS clearance [35]. In this study, the influence of CuB on ROS production in B16F10 cells was also evaluated. We found that NAC significantly diminished the anti-tumor effect of CuB on B16F10 cells. When NAC was present, the cell cycle progression of CuB-exposed cells was recovered, cell shape was retained as normal, plasma membrane blebbing was suppressed, cell migration was recovered, invasion ability was partially restored, and colony-forming ability was regained. More importantly, the G-actin pool was also restored to a relatively high level. Although CuB *per se* did not change ROS production in B16F10 cells, the ROS level was significantly decreased when cells were incubated with both CuB and NAC. Thus, the base level of ROS in B16F10 cells seems necessary for the anti-tumor and G-actin depletion activities of CuB.

In summary, our results indicated that CuB induces rapid depletion of the G-actin pool and the formation of actin aggregates in melanoma cells, which may at least partly account for its anti-tumor activity. The action of CuB might be dependent on the basal level of ROS since the suppression of ROS production with NAC markedly blocked the anti-tumor effect of CuB. Although the detailed pathway leading to the disruption of actin cytoskeleton by CuB remains to be clarified, our study provides a rationale for the development of CuB as a therapeutic agent against malignant melanomas.

## Funding

This work was supported by the grants from the Fundamental Research Funds for the Central Universities (21609403) and Major State Basic Research Development Program of China (2010CB833603).

## References

1 Farias MR, Schenkel EP, Mayer R and Rucker G. Cucurbitacins as constituents of *Wilbrandia ebracteata*. Planta Med 1993, 59: 272–275.
2 Peters RR, Farias MR and Ribeiro-do-Valle RM. Anti-inflammatory and analgesic effects of cucurbitacins from *Wilbrandia ebracteata*. Planta Med 1997, 63: 525–528.
3 Jayaprakasam B, Seeram NP and Nair MG. Anticancer and antiinflammatory activities of cucurbitacins from *Cucurbita andreana*. Cancer Lett 2003, 189: 11–16.
4 Peters RR, Baier Krepsky P, Siqueira-Junior JM, da Silva Rocha JC, Marques Bezerra M, de Albuquerque Ribeiro R and de Brum-Fernandes AJ, *et al*. Nitric oxide and cyclooxygenase may participate in the analgesic and anti-inflammatory effect of the cucurbitacins fraction from *Wilbrandia ebracteata*. Life Sci 2003, 73: 2185–2197.
5 Blaskovich MA, Sun J, Cantor A, Turkson J, Jove R and Sebti SM. Discovery of JSI-124 (cucurbitacin I), a selective Janus kinase/signal transducer and activator of transcription 3 signaling pathway inhibitor with potent antitumor activity against human and murine cancer cells in mice. Cancer Res 2003, 63: 1270–1279.
6 Wakimoto N, Yin D, O'Kelly J, Haritunians T, Karlan B, Said J and Xing H, *et al*. Cucurbitacin B has a potent antiproliferative effect on breast cancer cells *in vitro* and *in vivo*. Cancer Sci 2008, 99: 1793–1797.
7 Yin D, Wakimoto N, Xing H, Lu D, Huynh T, Wang X and Black KL, *et al*. Cucurbitacin B markedly inhibits growth and rapidly affects the cytoskeleton in glioblastoma multiforme. Int J Cancer 2008, 123: 1364–1375.
8 Haritunians T, Gueller S, Zhang L, Badr R, Yin D, Xing H and Fung MC, *et al*. Cucurbitacin B induces differentiation, cell cycle arrest, and actin cytoskeletal alterations in myeloid leukemia cells. Leuk Res 2008, 32: 1366–1373.
9 Thoennissen NH, Iwanski GB, Doan NB, Okamoto R, Lin P, Abbassi S and Song JH, *et al*. Cucurbitacin B induces apoptosis by inhibition of the JAK/STAT pathway and potentiates antiproliferative effects of gemcitabine on pancreatic cancer cells. Cancer Res 2009, 69: 5876–5884.
10 Liu T, Zhang M, Zhang H, Sun C and Deng Y. Inhibitory effects of cucurbitacin B on laryngeal squamous cell carcinoma. Eur Arch Otorhinolaryngol 2008, 265: 1225–1232.
11 Oh H, Mun YJ, Im SJ, Lee SY, Song HJ, Lee HS and Woo WH. Cucurbitacins from *Trichosanthes kirilowii* as the inhibitory components on tyrosinase activity and melanin synthesis of B16/F10 melanoma cells. Planta Med 2002, 68: 832–833.
12 Zhang M, Zhang H, Sun C, Shan X, Yang X, Li-Ling J and Deng Y. Targeted constitutive activation of signal transducer and activator of transcription 3 in human hepatocellular carcinoma cells by cucurbitacin B. Cancer Chemother Pharmacol 2009, 63: 635–642.
13 Chan KT, Li K, Liu SL, Chu KH, Toh M and Xie WD. Cucurbitacin B inhibits STAT3 and the Raf/MEK/ERK pathway in leukemia cell line K562. Cancer Lett 2010, 289: 46–52.
14 Zhang M, Sun C, Shan X, Yang X, Li-Ling J and Deng Y. Inhibition of pancreatic cancer cell growth by cucurbitacin B through modulation of signal transducer and activator of transcription 3 signaling. Pancreas 2010, 39: 923–929.
15 Yasuda S, Yogosawa S, Izutani Y, Nakamura Y, Watanabe H and Sakai T. Cucurbitacin B induces $G_2$ arrest and apoptosis via a reactive oxygen species-dependent mechanism in human colon adenocarcinoma SW480 cells. Mol Nutr Food Res 2010, 54: 559–565.
16 Nakashima S, Matsuda H, Kurume A, Oda Y, Nakamura S, Yamashita M and Yoshikawa M. Cucurbitacin E as a new inhibitor of cofilin phosphorylation in human leukemia U937 cells. Bioorg Med Chem Lett 2010, 20: 2994–2997.
17 Graness A, Poli V and Goppelt-Struebe M. STAT3-independent inhibition of lysophosphatidic acid-mediated upregulation of connective tissue growth factor (CTGF) by cucurbitacin I. Biochem Pharmacol 2006, 72: 32–41.
18 Liu T, Zhang M, Zhang H, Sun C, Yang X, Deng Y and Ji W. Combined antitumor activity of cucurbitacin B and docetaxel in laryngeal cancer. Eur J Pharmacol 2008, 587: 78–84.
19 Knecht DA, LaFleur RA, Kahsai AW, Argueta CE, Beshir AB and Fenteany G. Cucurbitacin I inhibits cell motility by indirectly interfering with actin dynamics. PLoS One 2010, 5: e14039.
20 Mansour M, Pohajdak B, Kast WM, Fuentes-Ortega A, Korets-Smith E, Weir GM and Brown RG, *et al*. Therapy of established B16-F10 melanoma tumors by a single vaccination of CTL/T helper peptides in VacciMax. J Transl Med 2007, 5: 20.
21 Ren SX, Ren ZJ, Zhao MY, Wang XB, Zuo SG and Yu F. Antitumor activity of endogenous mFlt4 displayed on a T4 phage nanoparticle surface. Acta Pharmacol Sin 2009, 30: 637–645.
22 Watts RG and Howard TH. Evidence for a gelsolin-rich, labile F-actin pool in human polymorphonuclear leukocytes. Cell Motil Cytoskeleton 1992, 21: 25–37.
23 Ji YH, Ji JL, Sun FY, Zeng YY, He XH, Zhao JX and Yu Y, *et al*. Quantitative proteomics analysis of chondrogenic differentiation of C3H10T1/2 mesenchymal stem cells by iTRAQ labeling coupled with on-line two-dimensional LC/MS/MS. Mol Cell Proteomics 2010, 9: 550–564.
24 Sun J, Blaskovich MA, Jove R, Livingston SK, Coppola D and Sebti SM. Cucurbitacin Q: a selective STAT3 activation inhibitor with potent antitumor activity. Oncogene 2005, 24: 3236–3245.
25 Shi X, Franko B, Frantz C, Amin HM and Lai R. JSI-124 (cucurbitacin I) inhibits Janus kinase-3/signal transducer and activator of transcription-3 signaling, downregulates nucleophosmin-anaplastic lymphoma kinase (ALK), and induces apoptosis in ALK-positive anaplastic large cell lymphoma cells. Br J Haematol 2006, 135: 26–32.
26 Duncan KL, Duncan MD, Alley MC and Sausville EA. Cucurbitacin E-induced disruption of the actin and vimentin cytoskeleton in prostate carcinoma cells. Biochem Pharmacol 1996, 52: 1553–1560.
27 Duncan MD and Duncan KL. Cucurbitacin E targets proliferating endothelia. J Surg Res 1997, 69: 55–60.
28 Maloney KN, Fujita M, Eggert US, Schroeder FC, Field CM, Mitchison TJ and Clardy J. Actin-aggregating cucurbitacins from *Physocarpus capitatus*. J Nat Prod 2008, 71: 1927–1929.
29 Momma K, Masuzawa Y, Nakai N, Chujo M, Murakami A, Kioka N and Kiyama Y, *et al*. Direct interaction of cucurbitacin E isolated from *Alsomitra macrocarpa* to actin filament. Cytotechnology 2008, 56: 33–39.
30 Pollard TD and Cooper JA. Actin, a central player in cell shape and movement. Science 2009, 326: 1208–1212.
31 Bershadsky AD, Gluck U, Denisenko ON, Sklyarova TV, Spector I and Ben-Ze'ev A. The state of actin assembly regulates actin and vinculin expression by a feedback loop. J Cell Sci 1995, 108: 1183–1193.
32 Insall RH and Machesky LM. Actin dynamics at the leading edge: from simple machinery to complex networks. Dev Cell 2009, 17: 310–322.
33 Bamburg JR and Wiggan OP. ADF/cofilin and actin dynamics in disease. Trends Cell Biol 2002, 12: 598–605.

34 Lazaro-Dieguez F, Aguado C, Mato E, Sanchez-Ruiz Y, Esteban I, Alberch J and Knecht E, *et al*. Dynamics of an F-actin aggresome generated by the actin-stabilizing toxin jasplakinolide. J Cell Sci 2008, 121: 1415–1425.

35 Meyskens FL, Jr, McNulty SE, Buckmeier JA, Tohidian NB, Spillane TJ, Kahlon RS and Gonzalez RI. Aberrant redox regulation in human metastatic melanoma cells compared to normal melanocytes. Free Radic Biol Med 2001, 31: 799–808.